This is a repository copy of *The tetrazole analogue of the auxin indole-3-acetic acid binds preferentially to TIR1 and not AFB5*.

White Rose Research Online URL for this paper:
http://eprints.whiterose.ac.uk/135235/

Version: Accepted Version

Article:

The tetrazole analogue of the auxin indole-3-acetic acid binds preferentially to TIR1 and not AFB5.

Mussa Quareshy [1†], **Justyna Prusinska** [1], **Martin Kieffer** [2], **Kosuke Fukui** [3], **Alonso J. Pardal** [1], **Silke Lehmann** [1,5], **Patrick Schafer** [1,5], **Charo I. del Genio** [1], **Stefan Kepinski** [2], **Kenichiro Hayashi** [3], **Andrew Marsh** [4], **Richard M. Napier** [1†]

[1] School of Life Sciences, University of Warwick, Coventry, CV4 7AL, UK

[2] Centre for Plant Sciences, University of Leeds, Leeds LS2 9JT

[3] Department of Biochemistry, Okayama University of Science, 1-1 Ridaicho, Kita-ku, Okayama-shi Okayama, JP 700-0005

[4] Department of Chemistry, University of Warwick, Coventry, CV4 7AL, UK

[5] Warwick Integrative Synthetic Biology Centre

[†] Corresponding authors:

mussaquareshy@gmail.com; Richard.napier@warwick.ac.uk

Highlights: We apply a functional group swap to auxin yielding an active auxin that also confers selectivity between 2 members of the auxin receptor family.

Key words: Auxin, bioisostere, herbicides, tetrazole, synthetic herbicides, rationale, drug-design, SAR, target selectivity.

Who did what: MQ came up with the concept of iMT, performed most of the experiments including synthesis of iMT in AM's lab with AM's guidance in designing the synthesis. JP performed the SPR SCK assays. MK performed the pull-down assays and SK provided the *tir1-1* knockout lines. KH and KF synthesised the 4,5 and 6 Cl iMT analogues as well as additional iMT, performed the *DR5::GUS* and *DII::VENUS* reporter assays. CIDG performed the curve fitting analysis to derive the primary root growth IC_{50} values. AJP, SL and PS performed the protoplast reporter assays and AJP did the qPCR. RN helped to develop the concept of iMT and was involved in the design of lead optimisation. MQ and RN wrote the manuscript with contributions from all the other authors.

29 **Abstract**

30 Auxin is considered one of the cardinal hormones in plant growth and development. It regulates a

31 wide range of processes throughout the plant. Synthetic auxins exploit the auxin-signalling pathway

32 and are valuable as herbicidal agrochemicals. Currently, despite a diversity of chemical scaffolds all

33 synthetic auxins have a carboxylic acid as the active core group. By applying bio-isosteric

34 replacement we discovered that indole-3-tetrazole was active by surface plasmon resonance (SPR)

35 spectrometry, showing that the tetrazole could initiate assembly of the TIR1 auxin co-receptor

36 complex. We then tested the tetrazole's efficacy in a range of whole plant physiological assays and in

37 protoplast reporter assays which all confirmed auxin activity, albeit rather weak. We then tested

38 indole-3-tetrazole against the AFB5 homologue of TIR1, finding that binding was selective against

39 TIR1, absent with AFB5. The kinetics of binding to TIR1 are contrasted to those for the herbicide

40 picloram, which shows the opposite receptor preference as it binds to AFB5 with far greater affinity

41 than to TIR1. The basis of the preference of indole-3-tetrazole for TIR1 was revealed to be a single

42 residue substitution using molecular docking, and assays using *tir1* and *afb5* mutant lines confirmed

43 selectivity *in vivo*. Given the potential that a TIR1-selective auxin might have for unmasking receptor-

44 specific actions, we followed a rational design, lead optimisation campaign and a set of chlorinated

45 indole-3-tetrazoles was synthesised. Improved affinity for TIR1 and the preference for binding to

46 TIR1 was maintained for 4- and 6-chloroindole-3-tetrazoles, coupled with improved efficacy *in vivo*.

47 This work expands the range of auxin chemistry for the design of receptor-selective synthetic auxins.

48

49

50

51

52

53

54

55

56

57

58

59 **Introduction**

60 Auxin (indole-3-acetic acid; IAA (1) Figure 1) regulates diverse developmental processes including

61 cell elongation, cell division, tropic responses, lateral rooting and branching, and synthetic auxins are

62 an important class of selective herbicides. The best-studied auxin receptor is the F-box protein

63 Transport Inhibitor Resistant 1 [1]. A wealth of experimentation has shown that TIR1 is the F-box

64 component of a Skp, Cullin, F-box (SCF) type E3 ubiquitin ligase complex SCF[TIR1], although it

65 wasn't until seminal work by two groups [2, 3] that TIR1 was shown to be the major auxin receptor.

66 The TIR1 family includes five additional Auxin F-Box proteins (AFBs) in *Arabidopsis* and activity

67 within this family has been shown to be largely redundant [4], with some notable exceptions. Root

68 architecture responses to nitrate levels appear to be mediated through AFB3 [5 6] and AFB5 has been

69 shown to be the dominant site of action for the picolinate herbicides [7 8].

70 The mechanism of auxin action is coordinated through transcriptional regulation and this has been

71 reviewed extensively [2, 3 9 10, 11]. At low auxin concentrations, AUX/IAA transcriptional repressor

72 proteins, together with co-repressor (TOPLESS) proteins repress genes targeted by the Auxin

73 Response Factor (ARF) transcriptional activators. As concentrations rise, auxin binds to TIR1

74 creating a high-affinity surface for recruitment of the AUX/IAA co-receptor. The assembly of this

75 SCF[TIR1]co-receptor complex has been used for an auxin binding assay using surface plasmon

76 resonance spectrometry [8, 12] . Assembly of the complex *in vivo* leads to ubiquination of the AUX/IAAs

77 and consequent degradation in the proteasome. The consequent reduction in concentrations of

78 AUX/IAA proteins releases the ARFs, allowing transcription to commence. The TIR1 crystal

79 structure [13] provided the paradigm for IAA acting as molecular glue between TIR1 and AUX/IAA,

80 and radiolabel and SPR binding experiments illustrated that the wide dynamic range of responses to

81 auxin may, in part, be accounted for by the range of affinities measured for different co-receptor

82 complexes [12, 14, 15].

83 The diversity of receptors suggests some differentiation of activity as well as dose dependence [5, 6 14].

84 It was of interest to pursue the selectivity found for picolinate herbicides and investigate the

85 possibility of receptor sub-class-specific ligands [16]. We have explored the tetrazole functional group

86 as a bioisostere (a chemical mimetic that sustains biologically activity) of carboxylic acids [17, 18] and

87 shown that indole-3-methyl tetrazole (compound 5, Figure 1; iMT) not only works as a weak auxin,

88 but that it binds selectively to TIR1, and not to AFB5. Rational design was shown to improve its

89 affinity for TIR1 without changing this selectivity.

90   **Results and Discussion**

91   <u>**Modelling alternative ligands for TIR1**</u>

92   Using the TIR1 crystal structure with IAA bound (PDB file 2P1P) we inspected the atomic distances

93   from the carboxylic oxygens of IAA to nearby residues and noted distances of 3.47Å to Arg_{403} and

94   4.52Å to Arg_{436} (Figure 2A). This indicated some exploitable space in this region and so we modelled

95   iMT (Figure 1) in the TIR1 site using the structure builder feature in Chimera [19] . Side-by-side

96   comparison of IAA with iMT (Figure 2 A & B) show the indole rings to be superimposable, with the

97   tetrazole group extending past the position of the carboxylic acid in IAA, further down into the

98   pocket. In our model the atomic distances were 1.89Å to Arg_{403} and 2.34Å to Arg_{436}. Furthermore,

99   the proximity of the Ser_{438} residue was also considered a probable hydrogen bonding partner for iMT

100   (Figure 2B).

101

102   <u>**Docking iMT into TIR1**</u>

103   Docking algorithms use more robust molecular force field calculations than a structure mutation in

104   Chimera and so iMT and IAA were docked using the Vina algorithm [20 21] into the auxin-binding

105   pocket of TIR1 using the coordinates from crystal structure 2P1Q (TIR1 with ligand and IAA7 degron

106   bound, but removed for docking). We reasoned that 2P1Q would be the most appropriate template for

107   docking in order to simulate the active state. Although there are no gross conformational changes

108   during binding [13], there are subtle side group moves implied from the different crystal datasets.

109   Docking predicted that the indole ring of bound iMT (scoring function -8.2 kcal/mol) would be

110   superimposed onto that for docked (scoring function -8.1 kcal/mol) and crystallographic IAA (Figure

111   2C), with a slight difference between alignments of the tetrazole and carboxylic acid. Interatomic

112   distances between the tetrazole and neighbouring arginines show 3 hydrogen bond donors within

113   range (Figure 2D). Thus *in silico* docking predicted that iMT would bind to TIR1, making it a non-

114   carboxylic acid auxin.

115

116   <u>**iMT binds TIR1 *in vitro* and acts as an auxin *in vivo***</u>

117   iMT was synthesised in a single step reaction from indole-3-acetonitrile with the addition of azide in a

118   cycloaddition reaction (Supporting Information Scheme 1; physicochemical properties are also

119   presented in Supporting Information Table 1). It was tested for binding to TIR1 using SPR. When

120   mixed with purified TIR1, iMT supported TIR1 co-receptor assembly on the SPR chip with an

121   activity of 18% relative to IAA (both at 50 μM; Figure 3A). We then used SPR to screen a selection

122   of other aromatic tetrazoles, including (2-(naphthalen-1-yl)tetrazole), the tetrazole equivalent of 1-

123   NAA (**11,** Supporting Information Figure 1). None of this collection of compounds bound to TIR1 or

124   AFB5, consistent with a lack of auxin activity in previous whole plant assays [22] [23].

125   It is notable that the SPR binding signal from iMT plateaued rapidly on both association and

126   dissociation phases (Figure 3A) unlike that for IAA, suggesting more rapid kinetics. Single cycle

127   kinetics recorded a K_D of 210 µM for iMT, compared to 5 µM for IAA (Table 1). The lower affinity

128   for iMT is contributed by a 15-fold faster off-rate constant than for IAA, and an almost 3-fold slower

129   on-rate constant.

130   The SPR assays are performed with TIR1 expressed in insect cells. In order to check activity with

131   plant-expressed TIR1, we tested the efficacy of iMT in pull-down assays with FLAG-tagged AtTIR1

132   expressed in *Nicotiana benthamiana* plus IAA7 peptide [24]. We observed a weak response compared to

133   IAA (Figure 3C), which is consistent with the SPR data on kinetic rates.

iMT lead optimisation

135   Whilst iMT has been shown to be an active auxin, it is considerably weaker than IAA and many other

136   synthetic auxins, and so rational design was applied to improve its activity. Past structure-activity

137   relationship studies for auxins have shown that the addition of chlorine at the 4 or 6 positions of IAA

138   yields potent auxins [25, 26, 27]. We also envisaged the chlorines might improve uptake properties [27].

139   Therefore, to start lead optimisation of iMT we synthesised the corresponding 4-, 5- and 6-

140   monochlorinated analogues (Supporting Information Scheme 2). Binding analysis using SPR showed

141   that 4-Cl-iMT did have enhanced binding to TIR1 (Figure 3A; Table 1. Addition of chlorine at the 6

142   position did not improve or reduce affinity and addition of Cl at the 5 position significantly decreased

143   affinity for TIR1 and reduced activity *in vivo* (Table 2).

Activity *in planta*.

145   Having established that iMT was active as an auxin in receptor binding assays, it was necessary to test

146   whether or not binding translated into auxin activity *in planta*. When *DR5::GUS* Arabidopsis

147   seedlings were grown on agar containing the test compound, iMT induced GUS activity at 50 µM,

148   compared to IAA which gave a signal at 1 µM (Figure 4A). We followed this up with the auxin

149   reporter *DII::VENUS* line [28] which showed a characteristic marked decrease in YFP signal in the

150   presence of IAA. Again, iMT showed an auxin-like response, but reduced compared to that of IAA

151   (Supporting Information Figure 2). Supporting these data, we treated 6-day-old *DR5::GFP* reporter

152   line seedlings with IAA or iMT and recorded the GFP signal from primary root tips after 2 and 24

153   hours (Figure 4B). After 2 hours only IAA induced the characteristic increase in GFP signal in the

154   epidermis, steele and the lateral root cap [29]. After 24 hours iMT-treated roots also showed an

155 enhanced GFP signal in cells types characteristic of auxin responses, although it remained weaker

156 than the IAA-induced signal (Figure 4B). We also noted responses to iMT analogues 4-Cl-iMT and 6-

157 Cl-iMT in the *DR5::GUS* assays (Figure 4A), in the *DII:VENUS* reporter assay (Supporting

158 Information Figure 2) and in the *DR5::GFP* assay at 24 hours, especially for 4-Cl-iMT (Figure 4B).

159 In order to reveal the timescale of responsiveness in live cells, we used a protoplast transient reporter

160 assay [30] adapted for use with auxin-sensitive promoters and automated to record continually (Figure

161 4C; Supporting Information Figure 3). A series of doses of IAA or 4Cl-iMT were applied in parallel

162 and the results indicated extended response lag times for iMT analogues compared to IAA, with

163 responses becoming evident only after about 2 hours. This is consistent with the DR5::GFP data

164 above (showing no response at 2 h) and might represent poor uptake kinetics for iMT and its

165 analogues. Nevertheless, a clear, auxin-dependent signal is generated as 4Cl-iMT accumulates.

166 **Root growth assays quantify auxin activity**

167 The genetic reporter assays provided evidence that iMT was an active auxin *in vivo* and showed

168 uptake of the compound into Arabidopsis roots and into protoplasts. However, genetic reporter assays

169 are difficult to quantify and so we conducted dose-response assays using seedling root growth

170 inhibition to evaluate IC_{50} values for each compound (Table 2). Defining the IC_{50} value as the

171 concentration of compound needed to reduce primary root growth to 50% of the length without

172 treatment, we obtained an IC_{50} value of 46 µM (±3) for iMT compared to 41 nM (±7) for IAA in Col-

173 0. We observed complete root growth inhibition at 300 µM for iMT compared with 11 µM for IAA

174 (Supporting Information Figure 4). The 1000-fold difference in activity *in vivo* is greater than the

175 difference in affinity observed for receptor binding (approximately 30-fold, Figure 3C). We noted

176 above that the response to iMT was slower than for IAA (Figure 4C), and these extended IC_{50} values

177 also suggest that uptake of iMT by plant cells is impaired affecting potency. Nevertheless, in the same

178 assay plates we observed increased lateral root density after iMT treatment, another characteristic

179 auxin response (Figure 5), and so iMT is acting positively as an auxin, and not by interfering with

180 selective elements of auxin physiology as reported for some other small molecules such as *cis*-

181 cinnamic acid and 3,4-(methylenedioxy)cinnamic acid [31, 32].

182

183 **iMT does not bind AFB5 and this can be explained using molecular docking**

184 In addition to testing iMT for binding to TIR1, we investigated binding to AFB5 (Figure 3B).

185 Somewhat surprisingly, we noted that iMT did not induce AFB5 co-receptor assembly, revealing a

186 selectivity towards TIR1. This is the opposite selectivity to that found for picloram and the 6-

187 arylpicolinate DAS534, which bind preferentially to AFB5 [7 8].

188   In order to investigate the basis of iMT's failure to bind to AFB5 we identified the residues lining the

189   auxin-binding pocket of each receptor [33]and aligned complementary sequences from AFB5 (Figure

190   6A). There are two key changes; His78 becomes an arginine, and Ser438 becomes an alanine in

191   AFB5. A change of histidine to arginine represents an increase in residue size and polarity, whilst a

192   change of serine to an alanine is a decrease in polarity, an increase in hydrophobicity and loss of a key

193   hydrogen bond acceptor. To understand how these changes might result in binding selectivity we

194   used the crystal structure of TIR1 (PDB file 2P1Q) and the homology model built for AFB5 from this

195   template [12] for docking *in silico* (Figure 6B to G). The His438Arg change is the most likely

196   contributing factor to iMT receptor selectivity. IAA docked into the AFB5 pocket in a favourable

197   pose, resembling that for TIR1, such that the aromatic ring is surrounded with hydrophobic residues

198   parallel to the base of the pocket, and the carboxylic acid is orientated towards arginine residues at the

199   base of the pocket, and towards the centre of the protein. Docking iMT into the AFB5 pocket

200   suggested that the increased steric bulk of the arginine displaced the tetrazole group upwards, with

201   this polar group now imposing on space previously taken by the alpha-carbon of IAA, and tilting the

202   pose of the indole ring with respect to the base of the pocket. Such a pose for iMT would be likely to

203   reduce favourable interactions with the AUX/IAA degron by perturbing the hydrophobic interactions

204   of auxin with the WPPV motif [13]. Binding analysis of the monochlorinated iMT analogues revealed

205   that binding remained selective for TIR1 with no binding to AFB5 (Figure 3; Table 1)

206   **Mutant Arabidopsis lines confirm that receptor specificity is maintained *in vivo*.**

207   In order to confirm that iMT is selective for TIR1 *in planta*, loss of function mutant lines of *A.*

208   *thaliana* were evaluated in the root growth assay using dose-response experiments (Supporting

209   Information Figure 4) In the *tir1-1* line we observed a shift in IC_{50} from 46 μM for iMT to 90 μM

210   (Table 2), and even at the highest dose of 300 μM primary root growth was not totally inhibited. With

211   *afb5-5* we observed no change in the IC_{50} value compared to wild type, consistent with the specificity

212   seen for iMT and TIR1 *in vitro*. Specificity is also apparent for the lateral root growth trait (Figure 5),

213   with the pattern of responsiveness to iMT being identical between Col-0 and *afb5-5*, but distinct from

214   *tir1-1*. Tests were extended to quantitative RT-PCR to evaluate responsiveness using widely used

215   auxin-responsive genes (Figure 4D). Treatment with IAA (1 μM) and 4-Cl-iMT (10 μM) gave similar

216   auxin-like responses in Col-0, but the response to 4-Cl-iMT was absent in *tir1-1* for all three reporter

217   genes, consistent with binding selectivity of 4-Cl-iMT for TIR1. The reporters *GH3.3* and *GH3.1*

218   gave partial responses to 4-Cl-iMT in *afb5-5*, whilst reporter *IAA5* responded as for IAA, as

219   anticipated for a line with a functional TIR1. Selectivity for TIR1 was also shown to be maintained

220   with lateral root density in the *tir1-1* line being significantly reduced compared to Col-0 and *afb5-5* at

221   the active higher dose rates (Figure 5,Table 2). Picloram demonstrated its inverse selectivity and

222   preference for AFB5 (Figure 5A).

223

Discussion

225   We have demonstrated that isosteric replacement of the carboxylic acid on IAA with a tetrazole yields

226   an active auxin that binds to the auxin receptor TIR1. Further, this isosteric change confers on iMT

227   selectivity for TIR1 which introduces the first auxin that does not engage with the receptor homologue

228   AFB5. Isosteric replacements have been reported for auxin previously, including the report of weak

229   activities in the *Avena* coleoptile extension and pea split epicotyl assays [22, 23], but never pursued. The

230   tetrazoles of 1-naphthylacetic acid and 2,4-dichlorophenoxyacetic acid were found to be far weaker

231   than iMT, as were other bioisosteres evaluated at the same time. Given the weak activity, perhaps it

232   is not surprising that no further interest has been shown in the 60 years since. However, with an SPR

233   binding assay, as well as Arabidopsis *TIR1/AFB* mutants, we were able to revisit the activity of non-

234   carboxylic synthetic auxins and this revealed target site specificity more extreme than the known

235   prefence of AFB5 for picloram and the picolinate auxins [7, 8]. This is the first report of a chemical tool

236   for examining receptor-selective responses and redundancy within the TIR1 family of receptors.

237   We have suggested the molecular basis of iMT specificity to be a histidine the base of the TIR1

238   binding pocket which is replaced by an arginine residue in AFB5 which protrudes more (Figure 6).

239   Without the crystal structure of the AFB5 receptor this explanation is based on a homology model [12],

240   although this remains a reasonable hypothesis until the AFB5 structure is solved. We recognise that

241   we have not represented the AFB2 clade in this study although it clusters close to TIR1 in sequence

242   alignments [4]. It is clear from all the data collected from *tir1-1* plants that the effects of iMT and 4-Cl-

243   iMT are dominated by recognition through TIR1. Nevertheless, we can't exclude some efficacy with

244   AFB2 and we note that at the relatively high concentrations needed for activity *in vivo* with this

245   current generation of iMT analogues there could be some cross-over signalling from other members

246   of the TIR1 family. Importantly, we now have chemical templates suitable for TIR1-dominant (iMT)

247   and AFB5-dominant (picolinate) activation of auxin signals. We do not yet fully understand the

248   significance of six redundant auxin receptors, but these compound families offer new tools to help

249   differentiate the receptors.

250   The tetrazole bioisostere iMT is not as potent as IAA, with a 40-fold poorer affinity for receptor

251   binding (Table 1). The difference in activity *in planta* is greater, perhaps due in part to reduced

252   uptake and transport. Some reduced uptake capacity is suggested in the timecourse of the protoplast

253   gene reporter assays (Figure 4C, Supporting Information Figure 2). Our initial lead optimisation

254   programme has yielded increased potency for 4-Cl-iMT with an IC_{50} value of 19 µM in the primary

255   root growth inhibition assay (Table 2). In terms of utility, we may compare this to picloram which is

256   a successful commercial herbicide. Picloram has an IC_{50} of 5 µM (Table 2). A further comparison

257   may be drawn to the herbicide glyphosate, which has an IC_{50} of 11 mM on its target enzyme 5-

258   enolpyruvylshikimate-3- phosphate synthase [34] and an IC_{50} on Arabidopsis rosettes of 50 μM, with

259   plants able to grow through treatments at 5 mM [35].

260   As with all agrochemicals, concerns are growing over resistance to current actives. The auxin family

261   of herbicides faces the same challenges. Resistance has not become a global threat [36, 37] but

262   applications are rising with the advent of dicamba- and 2,4-D-tolerant GM crops [38, 39]. However, as

263   well as maintaining the utility of the current arsenal, binding site variation might open the door to new

264   herbicide selectivities, wider or more restricted than the known broad-leaved dynamic of most current

265   compounds.

266

267

268 **Methods**

269 *In silico* modelling, chemical and protein visualisation

270 *In silico* modelling, molecular graphics and analyses were performed with the open source UCSF

271 Chimera package developed by the Resource for Biocomputing, Visualization, and Informatics at the

272 University of California, San Francisco (supported by NIGMS P41-GM103311). [19]. Marvin was used

273 for drawing, displaying and characterizing chemical structures, substructures and reactions. Calculator

274 Plugins were used for structure property prediction and calculation (Marvin v15.10.12.0, 2015;

275 ChemAxon (http://www.chemaxon.com). Chemical structures were drawn using ChemDraw

276 Professional v15.0.0.106. Docking was performed using an automated docking script [21] based on the

277 Vina algorithm [20]. Crystal structures 2P1P and 2P1Q [13] were sourced from RSCB [40].

278 Recombinant expression:

279 Expression constructs for both TIR1 and AFB5 were engineered to give fusion proteins His10-MBP-

280 (TEV)-FLAG-TIR1 and His-MBP-(TEV)-FLAG-AFB5 respectively and were coexpressed with

281 His10-(TEV)-ASK1 as descrbed in [8]. Generation of recombinant virus, quantification, selection,

282 expression screening, and generation of high-titer viral stock was done by Oxford Expression

283 Technologies (Oxford, U.K.). *Trichoplusia ni* (*T. ni High 5*) was used throughout as the host cell line

284 for expression. Cell densities were determined with a haemocytometer (Marienfeld, Neubauer-

285 improved 0.1mm, catalogue number: 0640030) using a 10x objective lens under a light microscope.

286 Cells were infected at a density of 1 x10^6 cells/mL with multiplicity of infection of 5. The cells were

287 harvested by centrifugation 72 h after infection and stored at -80°C.

288 Cell Lysis and protein extraction:

289 Frozen TIR1/ASK1 and AFB5/ASK1 pellets were thawed at room temperature and lysed for 40

290 minutes whist rolling at 4°C in Cytobuster™ Lysis medium (Invitrogen 5 mL per 250 mL of cell

291 lysate) supplemented with DNAse I (Roche), protease inhibitors (cOmplete™ Protease Inhibitor

292 Cocktail Tablets, Roche), 50 µM phytic acid (Sigma) and 1 mM reducing agent TCEP (Tris(2-

293 carboxyethyl)phosphine hydrochloride – Sigma). The lysate was diluted upto 30mL into Buffer A (20

294 mM Tris-HCl pH 7.4, 200 mM NaCl, 1mM EDTA, 50 µM phytic acid, 1 mM TCEP) and was

295 subjected to 3 x 30 seconds ultrasonication before centrifugation at 20,000 rpm at 4°C for 15 minutes.

296 The supernatant was then systematically filtered through 0.45 µm and 0.2 µm Whatman GD/X

297 syringe filters.

298

299

300   Protein purification:

301   The filtered lysate was loaded onto a nickel immobilised metal affinity chromatography column

302   (cOmplete His-Tag Purification Resin – Roche), washed with 10 column volumes of Buffer-A before

303   elution with Buffer-B (20 mM Tris-HCl pH 7.4, 200 mM NaCl, 1mM EDTA, 50 μM Phytic acid,1

304   mM TCEP, 250 mM Imidazole). TEV protease was added to the elute and incubated with mixing at

305   4^oC overnight. The solution was then loaded onto an anti-FLAG-affinity resin (ANTI-FLAG® M2

306   Affinity Gel - Sigma), washed with 10 column volumes of Buffer-C (10 mM HEPES pH7.4, 150 mM

307   NaCl, 3 mM EDTA, 50 uM Phytic acid, 1 mM TCEP, 0.05% Tween 20) and eluted with 3X-FLAG

308   peptide (Sigma) at 100ug/mL. Protein was stored on ice and protein concentrations were assayed by

309   nanodrop A_{280} nm measurement (Thermo Scientific).

310   SPR assays:

311   The auxin binding assays using SPR were done on a Biacore 2000 instrument as described previously

312   [8 41]. The kinetic analysis of iMT analogues was perfomed by single cycle kinetics on a Biacore T200,

313   titrating the compounds mixed with constant TIR1 before injection onto the SA chip. The orientation

314   of the assay was otherwise as for the Biacore 2000 assays, and degron peptide density on the chips

315   was controlled so that Rmax > 300 RU.

316   Pull-down assay:

317   The pull down assay was done according to the method described in [24]   where *Nicotiana*

318   *benthamiana* leaves were infiltrated with agrobacterium to express FLAG-TIR1 and leaf lysates were

319   incubated with biotynalted AUX/IAA7 degron (biotinyl-AKAQVVGWP PVRNYRKN) attached to

320   streptavidin beads. The reactions were done in the absence and presence of IAA or iMT at specified

321   concentrations.

322   Plant assays:

323   All root growth assays were done in Col-0 and mutants in this background, *tir1-1* and *afb5-5* lines [2 27],.

324   A series of plates with 15 serial dilutions for each compound was prepared in half strength Murashige

325   and Skoog medium. From the top concentration of 300 μM a three-fold dilution series was prepared,

326   plus a control without compound, giving a total of 16 plates.

327   From a pool of 6 day old seedlings a random selection of 10 were transferred onto each of the treated

328   plates and the position of the primary root tip was marked. The plates were placed randomly in the

329   stack such that the concentrations were not in order to account for positional bias. A plate with no

330   treatment was included in every assay for comparison with the lower end of the dose response

331   (longest roots) and as an indicator of reproducibility in the assay. The stack was placed with the

332   seedlings vertical for 6 days at 12 hour day (22 °C) 12 hour night (18 °C) cycles then scanned (HP

333   PSC 2500 series) at 1200 dpi in colour mode. Primary root growth from the marked point was

334   measured in Image J [42] and plotted using GraphPad Prism v 7.0.

335   The primary root growth measurements were fitted to a logistic function (2.1), using the Levenberg–

336   Marquardt algorithm, in QTI plot (IONDEV SRL, Romania, v 0.9.8.9) . The standard deviation of the

337   data points was weighted into the algorithm $f(x) = \frac{M}{1+e^{-k(x-x_0)}}$ where: M = Maximal value on curve,

338   e = natural logarithm, x_0 = IC_{50} value, k = Steepness of the curve.

339   Lateral root hairs were counted on screen and statistical comparisons were conducted in GraphPad

340   Prism v 7.0 using a two-way ANOVA looking at comparisons within each row (i.e. compound

341   concentration μM) and comparing columns (i.e. mutant lines) to a reference control column (i.e. WT

342   line), multiple comparisons reported to a 95% confidence level (Supporting Information Table 2).

343   *DR5::GUS* reporter assays:

344   5-days-old *DR5::GUS* seedlings were cultured in liquid MS medium (1.2% sucrose) with chemicals

345   for 16h at 23ºC. The seedlings were then washed with a GUS staining buffer [43] and transferred to a

346   GUS staining buffer containing 1 mM X-gluc. The seedlings were then incubated at 37 °C until

347   sufficient staining developed.

348   *DII::VENUS* assay:

349   5-day-old *DII::VENUS* seedlings [28] were cultured in liquid MS medium (1.2% sucrose) with 20 μM

350   yucasin, IAA biosynthesis inhibitor for 6h at 23ºC to accumulate DII-VENUS protein. The chemicals

351   were then added into culture medium at indicated concentration. After 1h incubation at 23 ºC in dark,

352   DII-VENUS image was captured by fluorescent microscopy BX-50 (Olympus, Japan) with YFP filter

353   sets.

354   *DR5::GFP* reporter assay:

355   Col-0 *DR5::GFP* seedlings [44] were germinated as above for root growth assays and used directly

356   from the plates. Seedlings from ther same batch of germinants were placed onto fresh media (half-

357   strength MS) prepared with compound from 100mM stocks in DMSO to give a final concentration of

358   50μM (final DMSO concentration of 0.05% v/v) in 6-well plates for 2 and 24 h in the dark.

359   Treatments were started simultaneously. At sampling, primary roots were cut to 3 cm, treated with 10

360   ug/ml Propidium Iodide, then placed onto a slide in water and imaged using a Leica (Germany) LSM

361   880 imaging system controlled by Leica Zen software with a 25 x oil immersion objective. GFP was

362   excited with a 488 nm laser line and detected between 499 nm and 544 nm. PI was excited with a 514

363   nm laser and detected between 598 nm and 720 nm. Control roots (DMSO 0.05% v/v) were used to

364   benchmark imaging settings and the same imaging parameters were used for both days, except for the

365   IAA treatment at 24 hours for which the gain was lowered to obtain a non-saturated image.

366

367   <u>Protoplast reporter assay:</u>

368   Mesophyll protoplast were obtained from leaf 8 of 4-week old plants following the "tape sandwich"

369   method using 4 plants per genotype [45]. The IAA5 promoter (At1g15580, 920 bp) was amplified from

370   genomic   Col-0   DNA   (primers

371   5'CCTGCAGGCTCTAGAGGATCCGCTGTCCATTATCACAAAGTC3'   and

372   5'TGTTTTTGGCGTCTTCCATGGCTTTGATGTTTTTGATTGAAAG3'). The backbone for the

373   pIAA5::LUC construct was generated from pFRK1::LUC (ABRC CD3-919) by digestion with

374   BamHI and NcoI and gel-purified. Backbone and PCR-amplified IAA5 promoter were combined in a

375   Gibson reaction using the CloneEZ kit (GenScript, USA). Plasmids containing the construct

376   *pGH3.3::LUC* [46] or *pIAA5::LUC* were transfected together with reporter *pUBQ10::GUS* for

377   normalisation [47]. After overnight incubation, protoplasts were treated with IAA or 4-Cl-iMT at the

378   concentrations described and LUC substrate luciferin added. The plate was immediately placed in a

379   Photek dark box and imaged with a photon-sensitive camera HRPCS218 (Photek; Supporting

380   Information Figure 4) for 6 h using the software Image32 (Photek) to integrate photon capture. After

381   imaging protoplasts were lysed for GUS activity analysis [46]. Images were processed with the Image32

382   software binning the photons captured for each minute into a time resolved image (TRI). Then, for

383   each well total intensity values were extracted. Light intensity was normalised to GUS activity.

384   <u>Quantitative RT-PCR</u>:

385   Leaf number 8 from 4-week old plants was syringe-infiltrated with either 1% DMSO in water (mock),

386   10 μM 4-Cl-iMT or 1 μM IAA for 3 hours. RNAs were extracted with RNeasy Plant Mini Kit

387   (Qiagen) and treated with TURBO[TM] DNase (Ambion) following manufacturer's instructions. For

388   cDNA synthesis 1 μg of RNA was reverse-trancribed with the SuperScript[TM] II Reverse Transcriptase

389   (Thermo Fisher Scientific), following manufacturer's specifications, using a primer for polyA tails

390   $d(T)_{19}$. qPCR was performed with SYBR® Green JumpStart[TM] Taq ReadyMixTM (Sigma), following

391   the manufacturer's recommendations (qPCR primers see Supporting information Table 3). All qPCR

392   primers were tested for efficiency on a standard curve. Three technical replicates were used for each

393   sample and 384-well plates were read using a CFX384 Touch[TM] Real-Time PCR Detection System

394   (Bio-Rad Laboratories). qPCR C_T values were exported into an excel file and analyzed using the

395   $\Delta\Delta C_T$ method [48]. Data was normalised to *UBC* (AT5G25760;[49]). *UBC* expression was found to be

396   stable under the conditions studied (Supporting information Figure 5).

Chemical synthesis:

iMTsynthesis via 1,3-dipolar cycloaddition [50] of sodium azide (NaN$_3$) and 2-(1H-indol-3-yl)acetonitrile with NaN$_3$, AlCl$_3$.THF in THF for 18h at 71˚C (Compound (1), Supporting Information Scheme 1 [51] [52]. 4-chloroindole-3-acetonitrile, 5-chloroindole-3-acetonitrile and 6-chloroindole-3-acetonitrile were synthesized according to the published procedure in [53], their corresponding 4/5/6 CL-iMT analougues were synthesised with the NH$_4$Cl, NaN$_3$ into DMF at 120˚C for 30h (Supporting Information Scheme 2). Complete methodologies including NMR and MS data are presented in the Supporting Information (Supporting Information Schemes 1 and 2).

412 <u>List of Supporting Information</u>

413 Scheme 1: Synthesis of iMT

414 Scheme 2: Synthesis of monochlorinated analogues of iMT

415 Table 1: Physiochemical properties of IAA and iMT analogues

416 Figure 1: Additional tetrazoles tested for auxin-like activity

417 Figure 2: Imaging of auxin responses using genetic reporter DII::VENUS

418 Figure 3: Protoplast activity assays

419 Figure 4: Root growth inhibition curves

420 Figure 5: *UBC* expression observation

421 Table 2: Two-way ANOVA for lateral root densities under 4-CL-iMT

422 Table 3: qPCR reference genes and primer sequences

423 This material is available free of charge via the internet at http://pubs.acs.org

424

425   END OF TEXT

426

427

428

429

430

431

432

433

434

435

436

References

438 1. Ruegger, M., Dewey, E., Gray, W. M., Hobbie, L., Turner, J., and Estelle, M. (1998) The TIR1
439   protein of Arabidopsis functions in auxin response and is related to human SKP2 and
440   yeast Grr1p, *Genes Dev. 12*, 198-207.
441 2. Dharmasiri, N., Dharmasiri, S., and Estelle, M. (2005) The F-box protein TIR1 is an auxin receptor,
442   *Nature 435*, 441-445.
443 3. Kepinski, S., and Leyser, O. (2005) The Arabidopsis F-box protein TIR1 is an auxin receptor,
444   *Nature 435*, 446-451.
445 4. Dharmasiri, N., Dharmasiri, S., Weijers, D., Lechner, E., Yamada, M., Hobbie, L., Ehrismann, J.
446   S., Jurgens, G., and Estelle, M. (2005) Plant development is regulated by a family of auxin
447   receptor F box proteins, *Dev. Cell 9*, 109-119.
448 5. Vidal, E. A., Moyano, T. C., Riveras, E., Contreras-Lopez, O., and Gutierrez, R. A. (2013) Systems
449   approaches map regulatory networks downstream of the auxin receptor AFB3 in the nitrate
450   response of Arabidopsis thaliana roots, *Proc. Natl. Acad. Sci. U. S. A. 110*, 12840-12845.
451 6. Roychoudhry, S., Kieffer, M., Del Bianco, M., Liao, C. Y., Weijers, D., and Kepinski, S. (2017)
452   The developmental and environmental regulation of gravitropic setpoint angle in Arabidopsis
453   and bean, *Sci. Rep. 7.*
454 7. Walsh, T. A., Neal, R., Merlo, A. O., Honma, M., Hicks, G. R., Wolff, K., Matsumura, W., and
455   Davies, J. P. (2006) Mutations in an Auxin Receptor Homolog AFB5 and in SGT1b Confer
456   Resistance to Synthetic Picolinate Auxins and Not to 2,4-Dichlorophenoxyacetic Acid or
457   Indole-3-Acetic Acid in Arabidopsis, *Plant Physiol. 142*, 542.
458 8. Lee, S., Sundaram, S., Armitage, L., Evans, J. P., Hawkes, T., Kepinski, S., Ferro, N., and Napier,
459   R. M. (2014) Defining Binding Efficiency and Specificity of Auxins for SCFTIR1/AFB-
460   Aux/IAA Co-receptor Complex Formation, *ACS Chem. Biol. 9*, 673-682.
461 9. Maraschin, F. D., Memelink, J., and Offringa, R. (2009) Auxin-induced, SCFTIR1-mediated poly-
462   ubiquitination marks AUX/IAA proteins for degradation, *Plant J. 59*, 100-109.
463 10. Stefanowicz, K., Lannoo, N., and Van Damme, E. J. M. (2015) Plant F-box Proteins - Judges
464   between Life and Death, *Crit. Rev. Plant Sci. 34*, 523-552.
465 11. Woodward, A. W., and Bartel, B. (2005) Auxin: Regulation, action, and interaction, *Ann. Bot.
466   (Oxford, U.K) 95*, 707-735.
467 12. Villalobos, L., Lee, S., De Oliveira, C., Ivetac, A., Brandt, W., Armitage, L., Sheard, L. B., Tan,
468   X., Parry, G., Mao, H. B., Zheng, N., Napier, R., Kepinski, S., and Estelle, M. (2012) A
469   combinatorial TIR1/AFB-Aux/IAA co-receptor system for differential sensing of auxin, *Nat.
470   Chem. Bio. 8*, 477-485.
471 13. Tan, X., Calderon-Villalobos, L. I. A., Sharon, M., Zheng, C. X., Robinson, C. V., Estelle, M.,
472   and Zheng, N. (2007) Mechanism of auxin perception by the TIR1 ubiquitin ligase, *Nature
473   446*, 640-645.
474 14. Pierre-Jerome, E., Moss, B. L., and Nemhauser, J. L. (2013) Tuning the auxin transcriptional
475   response, *J. Exp. Bot. 64*, 2557-2563.
476 15. Shimizu-Mitao, Y., and Kakimoto, T. (2014) Auxin Sensitivities of All Arabidopsis Aux/IAAs for
477   Degradation in the Presence of Every TIR1/AFB, *Plant Cell Physiol. 55*, 1450-1459.
478 16. Kapp, T. G., Rechenmacher, F., Neubauer, S., Maltsev, O. V., Cavalcanti-Adam, E. A., Zarka, R.,
479   Reuning, U., Notni, J., Wester, H. J., Mas-Moruno, C., Spatz, J., Geiger, B., and Kessler, H.
480   (2017) A Comprehensive Evaluation of the Activity and Selectivity Profile of Ligands for
481   RGD-binding Integrins, *Sci. Rep. 7.*
482 17. Lima, L. M. A., and Barreiro, E. J. (2005) Bioisosterism: A useful strategy for molecular
483   modification and drug design, *Curr. Med. Chem. 12*, 23-49.
484 18. Meanwell, N. A. (2011) Synopsis of Some Recent Tactical Application of Bioisosteres in Drug
485   Design, *J. Med. Chem. 54*, 2529-2591.
486 19. Pettersen, E. F., Goddard, T. D., Huang, C. C., Couch, G. S., Greenblatt, D. M., Meng, E. C., and
487   Ferrin, T. E. (2004) UCSF chimera - A visualization system for exploratory research and
488   analysis, *J. Comput. Chem. 25*, 1605-1612.

489   20. Trott, O., and Olson, A. J. (2010) Software News and Update AutoDock Vina: Improving the
490   Speed and Accuracy of Docking with a New Scoring Function, Efficient Optimization, and
491   Multithreading, *J. Comput. Chem 31*, 455-461.
492   21. Price, G. W., Gould, P. S., and Marsh, A. (2014) Use of Freely Available and Open Source Tools
493   for In Silico Screening in Chemical Biology, *J. Chem. Educ. 91*, 602-604.
494   22. van de Westeringh, C., and Veldstra, H. (1958) Researches on plant growth regulators, XXIV.
495   Structure/activity, IX. Tetrazole derivatives, *Rec.Trav.Chim.Pays-Bas 77*, 1107-1113.
496   23. Hamilton, R. H., Kivilaan, A., and McManus, J. M. (1960) Biological Activity of Tetrazole
497   Analogues of Indole-3-Acetic Acid and 2,4-Dichlorophenoxyacetic Acid, *Plant Physiol. 35*,
498   136.
499   24. Kepinski, S. (2009) Pull-Down Assays for Plant Hormone Research, In *Plant Hormones: Methods
500   and Protocols* (Cutler, S., and Bonetta, D., Eds.), pp 61-80, Humana Press, Totowa, NJ.
501   25. Katekar, G. F. (1979) Auxins: On the nature of the receptor site and molecular requirements for
502   auxin activity, *Phytochemistry 18*, 223-233.
503   26. Katekar, G. F., and Geissler, A. E. (1982) Auxins II: The effect of chlorinated indolylacetic acids
504   on pea stems, *Phytochemistry 21*, 257-260.
505   27. Simon, S., Kubes, M., Baster, P., Robert, S., Dobrev, P. I., Friml, J., Petrasek, J., and Zazimalova,
506   E. (2013) Defining the selectivity of processes along the auxin response chain: a study using
507   auxin analogues, *New Phytol. 200*, 1034-1048.
508   28. Brunoud, G., Wells, D. M., Oliva, M., Larrieu, A., Mirabet, V., Burrow, A. H., Beeckman, T.,
509   Kepinski, S., Traas, J., Bennett, M. J., and Vernoux, T. (2012) A novel sensor to map auxin
510   response and distribution at high spatio-temporal resolution, *Nature 482*, 103-U132.
511   29. Overvoorde, P., Fukaki, H., and Beeckman, T. (2010) Auxin Control of Root Development, *Cold
512   Spring Harbor Perspect. Biol. 2*.
513   30. Niu, Y., and Sheen, J. (2012) Transient Expression Assays for Quantifying Signaling Output, In
514   *Plant Signalling Networks: Methods and Protocols* (Wang, Z.-Y., and Yang, Z., Eds.), pp
515   195-206, Humana Press, Totowa, NJ.
516   31. Steenackers, W., Cesarino, I., Klima, P., Quareshy, M., Vanholme, R., Corneillie, S., Kumpf, R.
517   P., Van de Wouwer, D., Ljung, K., Goeminne, G., Novak, O., Zazimalova, E., Napier, R.,
518   Boerjan, W., and Vanholme, B. (2016) The Allelochemical MDCA Inhibits Lignification and
519   Affects Auxin Homeostasis, *Plant Physiol. 172*, 874-888.
520   32. Steenackers, W., Klima, P., Quareshy, M., Cesarino, I., Kumpf, R. P., Corneillie, S., Araujo, P.,
521   Viaene, T., Goeminne, G., Nowack, M. K., Ljung, K., Friml, J., Blakeslee, J. J., Novak, O.,
522   Zazimalova, E., Napier, R., Boerjan, W., and Vanholme, B. (2017) cis-Cinnamic Acid Is a
523   Novel, Natural Auxin Efflux Inhibitor That Promotes Lateral Root Formation, *Plant Physiol.
524   173*, 552-565.
525   33. Uzunova, V. V., Quareshy, M., del Genio, C. I., and Napier, R. M. (2016) Tomographic docking
526   suggests the mechanism of auxin receptor TIR1 selectivity, *Open Biol. 6*.
527   34. Funke, T., Han, H., Healy-Fried, M. L., Fischer, M., and Schonbrunn, E. (2006) Molecular basis
528   for the herbicide resistance of Roundup Ready crops, *Proc. Natl. Acad. Sci. U. S. A. 103*,
529   13010-13015.
530   35. Tian, Y. S., Xu, J., Xiong, A. S., Zhao, W., Fu, X. Y., Peng, R. H., and Yao, Q. H. (2011)
531   Improvement of Glyphosate Resistance through Concurrent Mutations in Three Amino Acids
532   of the Ochrobactrum 5-Enopyruvylshikimate-3-Phosphate Synthase, *Appl. Environ.
533   Microbiol.77*, 8409-8414.
534   36. Mithila, J., Hall, J. C., Johnson, W. G., Kelley, K. B., and Riechers, D. E. (2011) Evolution of
535   Resistance to Auxinic Herbicides: Historical Perspectives, Mechanisms of Resistance, and
536   Implications for Broadleaf Weed Management in Agronomic Crops, *Weed Sci. 59*, 445-457.
537   37. Busi, R., Goggin, D. E., Heap, I. M., Horak, M. J., Jugulam, M., Masters, R. A., Napier, R. M.,
538   Riar, D. S., Satchivi, N. M., Torra, J., Westra, P., and Wright, T. R. (2017) Weed resistance to
539   synthetic auxin herbicides, *Pest Manage. Sci. Epub 13 December 2017
540   https://doi.org/10.1002/ps.4823*.
541   38. Behrens, M. R., Mutlu, N., Chakraborty, S., Dumitru, R., Jiang, W. Z., LaVallee, B. J., Herman, P.
542   L., Clemente, T. E., and Weeks, D. P. (2007) Dicamba resistance: Enlarging and preserving
543   biotechnology-based weed management strategies, *Science 316*, 1185-1188.

544   39. Wright, T. R., Shan, G. M., Walsh, T. A., Lira, J. M., Cui, C., Song, P., Zhuang, M. B., Arnold, N.
545   L., Lin, G. F., Yau, K., Russell, S. M., Cicchillo, R. M., Peterson, M. A., Simpson, D. M.,
546   Zhou, N., Ponsamuel, J., and Zhang, Z. Y. (2010) Robust crop resistance to broadleaf and
547   grass herbicides provided by aryloxyalkanoate dioxygenase transgenes, *Proc. Natl. Acad. Sci.*
548   *U. S. A. 107*, 20240-20245.
549   40. Berman, H. M., Westbrook, J., Feng, Z., Gilliland, G., Bhat, T. N., Weissig, H., Shindyalov, I. N.,
550   and Bourne, P. E. (2000) The Protein Data Bank, *Nucleic Acids Res. 28*, 235-242.
551   41. Quareshy, M., Uzunova, V., Prusinska, J. M., and Napier, R. M. (2017) Assaying Auxin Receptor
552   Activity Using SPR Assays with F-Box Proteins and Aux/IAA Degrons, In *Plant Hormones:*
553   *Methods and Protocols* (Kleine-Vehn, J., and Sauer, M., Eds.), pp 159-191, Springer New
554   York, New York, NY.
555   42. Schneider, C. A., Rasband, W. S., and Eliceiri, K. W. (2012) NIH Image to ImageJ: 25 years of
556   image analysis, *Nat. Methods 9*, 671-675.
557   43. Yamazoe, A., Hayashi, K., Kepinski, S., Leyser, O., and Nozaki, H. (2005) Characterization of
558   terfestatin A, a new specific inhibitor for auxin signaling, *Plant Physiol. 139*, 779-789.
559   44. Ottenschlager, I., Wolff, P., Wolverton, C., Bhalerao, R. P., Sandberg, G., Ishikawa, H., Evans,
560   M., and Palme, K. (2003) Gravity-regulated differential auxin transport from columella to
561   lateral root cap cells, *Proc. Natl. Acad. Sci. U. S. A. 100*, 2987-2991.
562   45. Wu, F. H., Shen, S. C., Lee, L. Y., Lee, S. H., Chan, M. T., and Lin, C. S. (2009) Tape-
563   Arabidopsis Sandwich - a simpler Arabidopsis protoplast isolation method, *Plant Methods 5*.
564   46. Yoo, S. D., Cho, Y. H., and Sheen, J. (2007) Arabidopsis mesophyll protoplasts: a versatile cell
565   system for transient gene expression analysis, *Nat. Protoc. 2*, 1565-1572.
566   47. Norris, S. R., Meyer, S. E., and Callis, J. (1993) The intron of arabidopsis-thaliana polyubiquitin
567   genes is conserved in location and is a quantitative determinant of chimeric gene-expression,
568   *Plant Mol. Biol. 21*, 895-906.
569   48. Livak, K. J., and Schmittgen, T. D. (2001) Analysis of relative gene expression data using real-
570   time quantitative PCR and the 2(T)(-Delta Delta C) method, *Methods 25*, 402-408.
571   49. Czechowski, T., Stitt, M., Altmann, T., Udvardi, M. K., and Scheible, W. R. (2005) Genome-wide
572   identification and testing of superior reference genes for transcript normalization in
573   Arabidopsis, *Plant Physiol. 139*, 5-17.
574   50. Wittenberger, S. J. (1994) Recent developments in tetrazole chemistry - A review, *Org. Prep.*
575   *Proced. Int. 26*, 499-531.
576   51. Dolusic, E., Larrieu, P., Moineaux, L., Stroobant, V., Pilotte, L., Colau, D., Pochet, L., Van den
577   Eynde, B., Masereel, B., Wouters, J., and Frederick, R. (2011) Tryptophan 2,3-Dioxygenase
578   (TDO) Inhibitors. 3-(2-(Pyridyl)ethenyl)indoles as Potential Anticancer Immunomodulators,
579   *J. Med. Chem. 54*, 5320-5334.
580   52. McManus, J. M., and Herbst, R. M. (1959) Tetrazole Analogs of Aminobenzoic Acid Derivatives,
581   *J. Org. Chem. 24*, 1044-1046.
582   53. Katayama, M. (2000) Synthesis and biological activities of 4-chloroindole-3-acetic acid and its
583   esters, *Biosci., Biotechnol., Biochem. 64*, 808-815.

584

Tables:

Compound	TIR1					AFB5				
	ka (1/Ms)	± (fit error)	kd (1/s)	± (fit error)	KD (μM)	ka (1/Ms)	± (fit error)	kd (1/s)	± (fit error)	KD (μM)
IAA	8.06E+02	3.4	3.85E-03	9.60E-06	4.78	4.61E+02	6	7.02E-02	4.50E-04	154
iMT	3.04E+02	3.2	6.39E-02	1.40E-04	210	-	-	-	-	-
4-Cl-iMT	2.43E+02	1.8	3.82E-02	1.90E-04	157	-	-	-	-	-
5-Cl-iMT	3.28E+02	8.8	1.20E-01	5.30E-04	366	-	-	-	-	-
6-Cl-iMT	3.75E+02	4.7	7.64E-02	2.20E-04	204	-	-	-	-	-

Table 1. Kinetic binding data.
The Biacore T200 single cycle kinetic facility was used with titrations of each compound against constant receptor concentration to derive kinetic values for each compound.

| | A. thaliana lines (IC$_{50}$ values in µM) | | | | | | |
Compound	Col-0	± SE	*tir1-1*	± SE	*afb5-5*	± SE	Sensitivity
IAA	0.04	-0.01	0.06	-0.01	0.03	-0.01	-
4-Cl-IAA	0.04	-0.004	-	-	-	-	-
5-Cl-IAA	0.19	-0.01	-	-	-	-	-
6-Cl-IAA	0.02	-0.002	-	-	-	-	-
Picloram	4.79	-0.87	8.4	-0.84	43.66	-6.37	AFB5
iMT	46.21	-2.87	90.61	-6.99	45.59	-4.9	TIR1
4 Cl iMT	19.05	-1.96	36.91	-3.92	19.12	-3.39	TIR1
5 Cl iMT	59.47	-6.85	55.04	-4.29	-	-	-
6 Cl iMT	32.48	-1.25	34.82	-2.17	28.09	-1.71	TIR1

Table 2: iMT analogues are active as auxins in the Arabidopsis primary root growth inhibition assay.
The IC$_{50}$ values (±SE) for the inhibition of primary root growth were calculated from statistical fits to dose response data. Receptor preferences are noted on the right.

1
2
3 Figures:
4
5
6
7
8
9
10
11
12
13
14
15
16
17
18
19
20
21
22
23
24
25
26
27
28

A

Structure	Name	R1	R2	R3	R4
1	IAA	H	H	H	H
2	4-Cl-IAA	Cl	H	H	H
3	5-Cl-IAA	H	Cl	H	H
4	6-Cl-IAA	H	H	Cl	H

Structure	Name	R1	R2	R3	R4
5	iMT	H	H	H	H
6	4-Cl-iMT	Cl	H	H	H
7	5-Cl-iMT	H	Cl	H	H
8	6-Cl-iMT	H	H	Cl	H
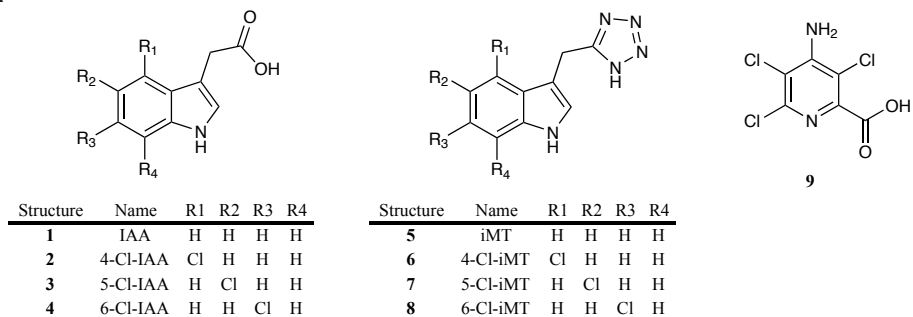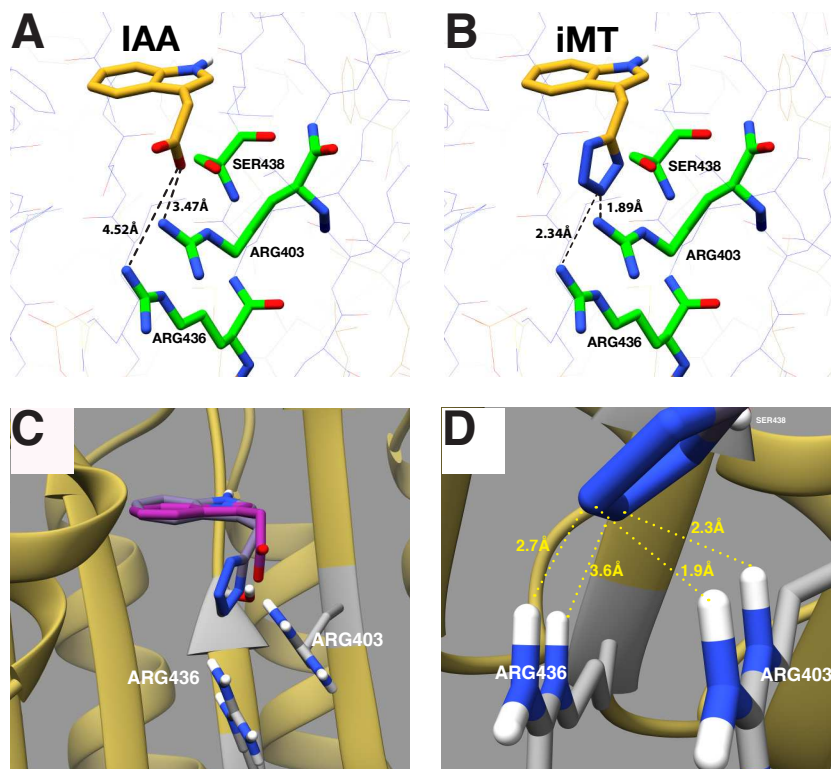
Figur
Chem
analo

Figure 2. Modelling iMT as a ligand for TIR1.
A: The crystal structure of IAA (gold) bound in the TIR1 receptor, with key residues shown with coloured heteroatoms. Interatomic distances are shown as dashed black lines. B: As A, but with the tetrazole analogue modelled in the binding site using Chimera. C: IAA (magenta) and iMT (grey), each docked (AutoDock Vina) in the deep binding pocket of TIR1 (gold, ribbon). The docked poses are consistent with the modelling in B. The indole ring of iMT adopts the same plane as that for IAA (which is the same as that seen in the crystal structure), with the tetrazole group projecting past the carboxylic acid group of IAA. D: shows the atomic distances between the tetrazole group nitrogens and neighbouring arginine residues.
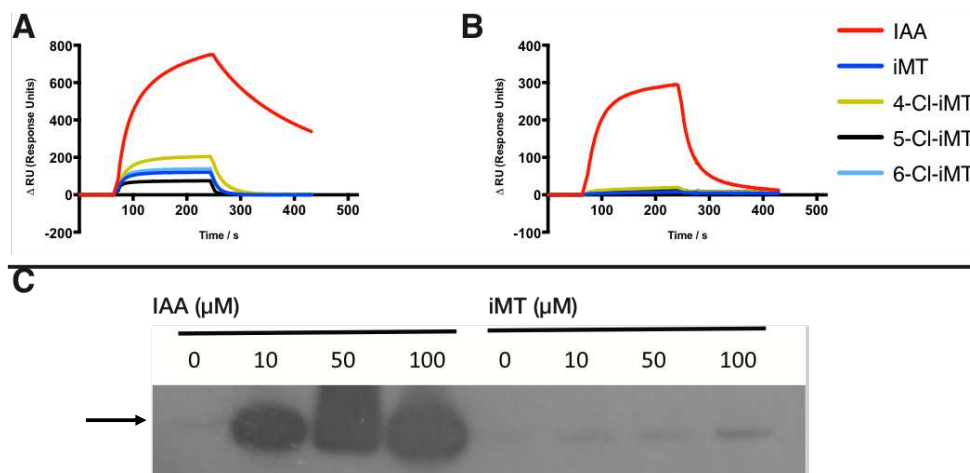
Figure 3. iMT binds to TIR1, but not to AFB5.
SPR binding curves for compounds screened at 50μM against TIR1 (Panel A) and AFB5 (Panel B). In each case IAA (red trace) is used for reference. With TIR1 we observe a saturating binding response with a rapid off rate for all iMT analogues. None of the iMT analogues were active against AFB5. C: A pull-down assay for FLAG-TIR1 in the presence of increasing concentrations of IAA (left) and iMT (right). A western blot developed with anti-FLAG antibody detects FLAG-TIR1 (arrow) bound to streptavidin-coated beads loaded with biotinylated degron peptide. As with SPR, there is a strong response with IAA, and the iMT response is dose-dependent, but weaker.
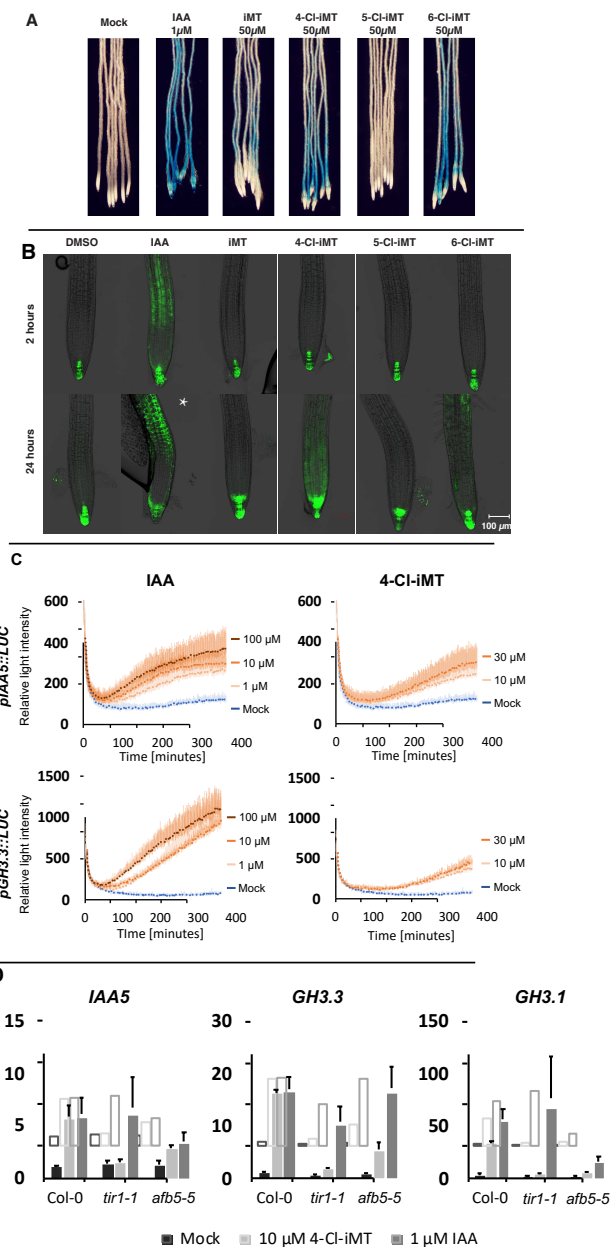
Figure 4. iMT analogues are active auxins in vivo.

A: The DR5::GUS reporter line indicates auxin activity of iMT and its monochlorinated analogues. Treatments were for 16 h at 1µM for IAA, 50 µM for iMT and its analogues. No activity was seen with 5-Cl-iMT. B: Signals from DR5::GFP after 2 and 24 hours of treatment. Activity is seen after 2 hours with IAA, iMT and 4- and 6-Cl-iMT show activity within 24 hours, with 4-Cl-iMT giving a comparatively strong response. *For the image of IAA treatment after 24 hours the gain was lowered to avoid a saturated signal. C: Arabidopsis protoplasts were transformed with auxin-sensitive reporter constructs pGH3.3::LUC (above) or pIAA5::LUC (below) before treatment with IAA (left) or 4-Cl-iMT (right), each over responsive dose ranges and each with a mock treatment (blue). Luciferase activity was recorded each minute for 6 hours. Error bars represent standard deviations of technical replicates and the plots are a representative set from three biological repeats. D: Quantitative PCR data for three auxin-responsive reporter genes, *IAA5*, *GH3.3* and *GH3.1*. RNA samples were prepared from treated leaf tissues collected 3 hours after treatment with mock, 4-Cl-iMT or IAA (10 and 1 µM respectively) from Col-0, *tir1-1* and *afb5-5* lines. Error bars represent the standard error of the mean of biological repeats (n = 4).
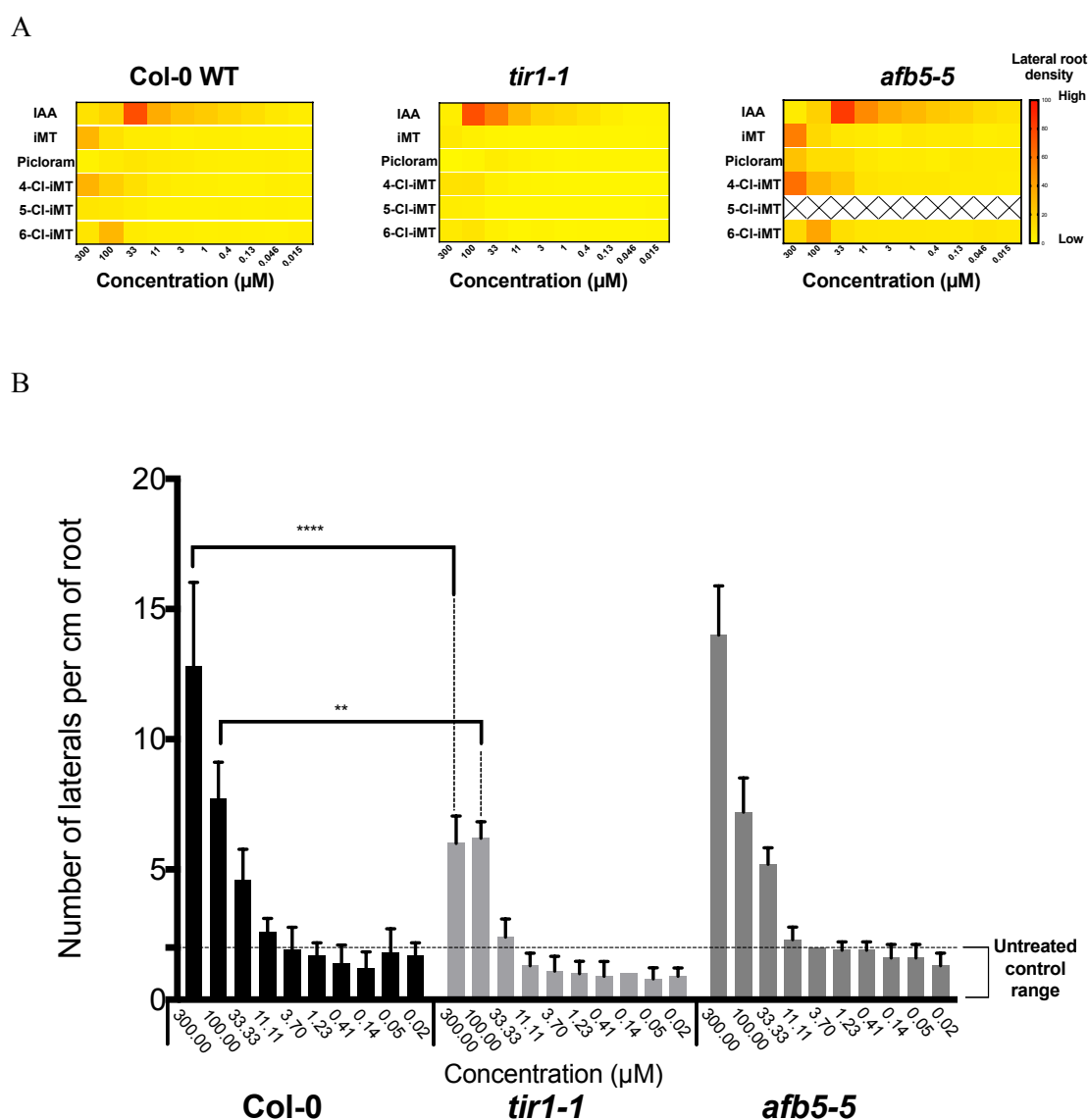
A

B

Figure 5: The *tir1-1* mutant is insensitive to iMT and 4-Cl-iMT

A: Normalised Lateral root densities plotted as heat maps to display the effects of compound and compound concentration for wild type, *tir1-1* and *afb5-5* knockout lines. Lateral root density is reduced in the *tir1-1* mutant challenged with iMT, 4-Cl-iMT and 6-Cl-iMT, but not in *afb5-5* nor Col-0. Cross-hatching (XX) indicates that this was not tested. B: From the same data as A but focussing on lateral root densities for lines treated with 4-Cl-iMT. Error bars indicate +/- the standard error of the means. A two-way ANOVA was used to compare densities at each concentration for each mutant line versus Col-0; ** P≤0.01 and **** is for P≤0.0001 using 10 replicates per concentration per seed line. The loss of density at higher concentrations is seen only with *tir1-1* and not in the *afb5-5* line.
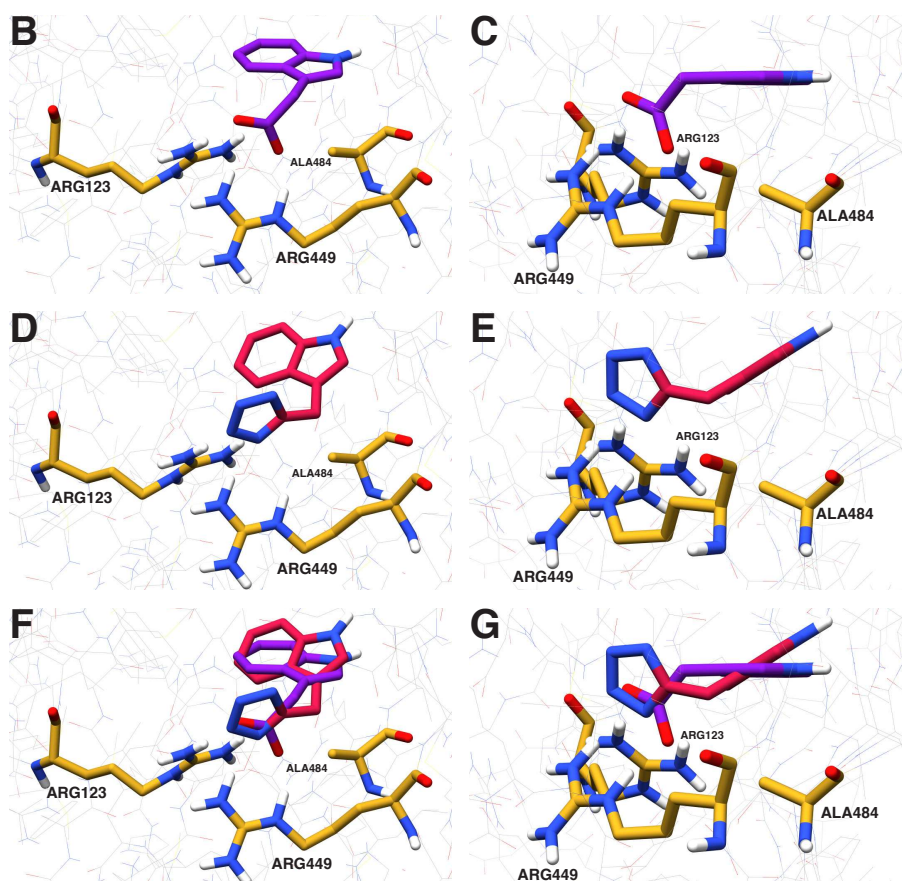
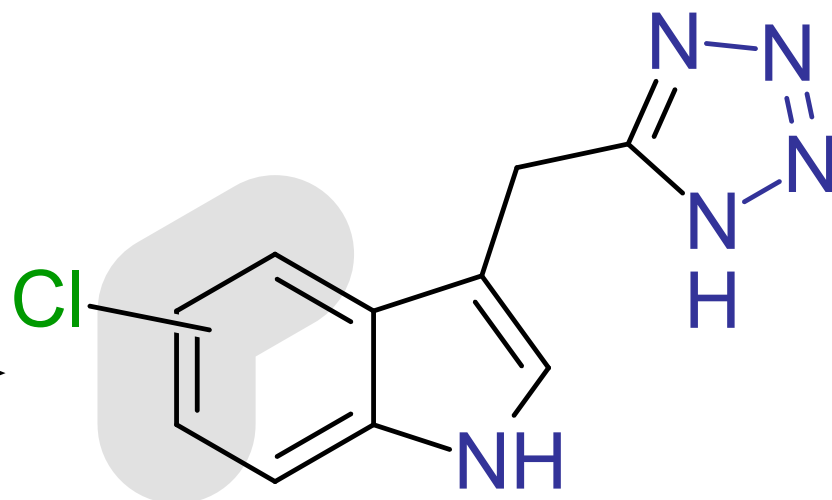**Figure 6. A model for iMT selectivity based on space constraints in AFB5.**
A: The binding pocket residues of TIR1 are alligned against those of AFB5, using the residue numbers for TIR1 (Clustal 2.1). Key differences are highlighted in yellow and include His78, which is Arg in AFB5, and S438 Ala in AFB5. **B – G: Views of the homology model for AFB5** (Calderon-Villalobos et al., 2012) showing IAA (B and C) or iMT (D and E), or both F and G) docked using AutoDock Vina.   The views in each left hand panel are similar to those for TIR1 in Figure 1, and on the right views are revolved to show the pose of the side group out of the plane of the aromatic ring system**.** Note that iMT does not adopt the same pose as IAA in AFB5 because the space occupied by the tetrazole in TIR1 (Figure 1) is partially occupied by Arg123 in AFB5, forcing the tetrazole up and away from the base of the pocket, resulting in the indole twisting from alignment with the base of the pocket.
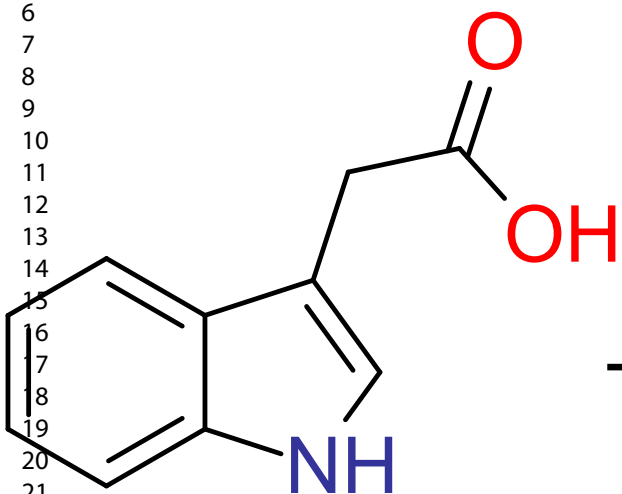
TIR1 binding ✔

AFB5 binding ✔

TIR1 binding ✔

AFB5 binding ✖